Lab on a Chip

Accepted Manuscript

ROYAL SOCIETY OF CHEMISTRY

www.rsc.org/loc

Cite this: DOI: 10.1039/c0xx00000x

www.rsc.org/xxxxxx

PAPER

From cellular lysis to microarray detection, an integrated thermoplastic elastomer (TPE) point of care Lab on a Disc

Emmanuel Roy,*[a] Gale Stewart,[b] Maxence Mounier,[a] Lidija Malic,[a] Régis Peytavi,[b] Liviu Clime,[a] Marc Madou,[c] Maurice Bossinot,[b] Michel G. Bergeron,[b] and Teodor Veres*[a]

Received (in XXX, XXX) Xth XXXXXXXXX 20XX, Accepted Xth XXXXXXXXX 20XX
DOI: 10.1039/b000000x

We present an all-thermoplastic integrated sample-to-answer centrifugal microfluidic Lab-on-Disc system (LoD) for nucleic acid analysis. The proposed CD system and engineered platform were employed for analysis of *Bacillus atrophaeus* subsp. *globigii* spores. The complete assay comprised cellular lysis, polymerase chain reaction (PCR) amplification, amplicon digestion, and microarray hybridization on a plastic support. The fluidic robustness and operating efficiency of the assay were ensured through analytical optimization of microfluidic tools enabling beneficial implementation of capillary valves and accurate control of all flow timing procedures. The assay reliability was further improved through the development of two novel microfluidic strategies for reagents mixing and flow delay on the CD platform. In order to bridge the gap between the proof-of-concept LoD and production prototype demonstration, low-cost thermoplastic elastomer (TPE) was selected as the material for CD fabrication and assembly, allowing the use of both, high quality hot-embossing and injection molding processes. Additionally, the low-temperature and pressure-free assembly and bonding properties of TPE material offer a pertinent solution for simple and efficient loading and storage of reagents and other on-board components. This feature was demonstrated through integration and conditioning of microbeads, magnetic discs, dried DNA buffer reagents and spotted DNA array inserts. Furthermore, all microfluidic functions and plastic parts were designed according to the current injection mold-making knowledge for industrialization purposes. Therefore, the current work highlights a seamless strategy that promotes a feasible path for the transfer from prototype toward realistic industrialization. This work aims to establish the full potential for TPE-based centrifugal system as a mainstream microfluidic diagnostic platform for clinical diagnosis, water and food safety, and other molecular diagnostic applications.

1. Introduction

Over the last decade, the development of integrated and low-cost point-of-care (POC) devices for rapid diagnostics has been fuelled by the miniaturisation and automation of the analytical protocols based on microfluidics. The obvious advantages of microfluidics include reduced sample and reagents consumption, enhanced efficiency and fast reaction times with potential for integration and multiplexing.[1,2,3] The maturity and ultimately, the success of microfluidics in POC applications will largely depend on the ability to integrate multiple operations into a monolithic device. However, moving from simple stand-alone microfluidic devices to a complete microfluidic POC system that implements a complex sample-to-answer bio-assay protocol is challenging. Specifically for POC applications, further improvements are required for the integration of microfluidic functions, on-chip reagent storage and the reduction of fabrication costs, in addition to the bio-assay adaptation to a microfluidic format itself. Several POC systems have been developed and marketed for analysis of blood gases, blood electrolytes and certain protein biomarkers, such as the Piccolo® from Abaxis Inc., and the iStat® from Abbott Inc.. However, these devices do not meet the current demand for clinical diagnosis based on DNA and RNA signatures. Furthermore, POC integration of complex genomic-based diagnostic assays is challenging due to the PCR amplification that is involved, the large number of steps involved and potential contamination and instability issues.[4] A few commercial microfluidic platforms for genomic analysis such as Handylab's cartridge and Cepheid's GeneXpert have successfully integrated several, but not all, assay steps in a single device. For instance, Handylab Inc. developed a microfluidic thermocycling cartridge for the detection of *group B Streptococcus*, *Clostridium difficile* and methicillin resistant *S.*

[a] *Life Sciences Division, National Research Council of Canada, 75 Boul. de Mortagne, Boucherville, J4B 6Y4, Québec, Canada.*
[b] *Centre de Recherche en Infectiologie, Université Laval, 2705 Boul. Laurier, Sainte-Foy, G1V 4G3, Québec, Canada.*
[c] *Department of Mechanical and Aerospace Engineering, University of California, Irvine, CA, USA*
Corresponding author :
Emmanuel.roy@nrc.gc.ca and Teodor.veres@nrc.gc.ca
† Electronic Supplementary Information (ESI) available: See DOI: 10.1039/b000000x/

aureus (MRSA). However, a number of procedures are performed off-chip, such as bacterial cell lysis and nucleic acid purification. Similarly, the GeneXpert®, which relies on real-time amplification for detection, still requires certain off-chip reagent manipulations, including mixing and incubation. While these systems constitute a significant advancement over traditional genomic laboratory assays, the requirement for off-chip manual procedures reinforces the continued need for a fully integrated assay.

In this paper, we demonstrate a microfluidic system capable of a complete nucleic acid (NA) assay. Instead of real time PCR amplification, the platform presented here features PCR amplification coupled with NA microarray fluorescent detection on a customizable polymer microarray insert. Among the numerous microfluidic technologies available, we decided to design a centrifugal microfluidic system, initially conceptualized by Anderson *et al.*[5,6,7] in the late 60's. We chose centrifugal liquid manipulation for its simplicity, robustness and enriched liquid propulsion and valving means.[8,9] While integrated lab-on-disc platforms have already been demonstrated for biochemistry and immunoassays from whole blood[10] and the capability of LoD platforms for real time PCR,[11] cell lysing,[12] and DNA micro-array hybridization[13,14] were previously reported, none of these systems demonstrated a complete sample-to-answer integration. To achieve this, in the present work, all the required microfluidic functions for the execution of the complete assay protocol have been integrated in a simple and rapid-to-fabricate polymer-based LoD device controlled by a custom-made hardware platform.

The engineered platform driving the LoD allowed for spinning, positioning, active magnetic lysing, fluid mixing, active pinch valving and included several Peltier-based heating elements required for the inactivation of inhibitors and PCR. The implementation of the analytical protocol is based on the use of both capillary and active pinch valves together with two novel strategies for passive mixing and liquid flow control for centrifugal microfluidics. New analytical tools that allow for accurate design and implementation of capillary valves based on either hydrophobic or hydrophilic surfaces are also presented.

Through the complete integration of a molecular assay for *Bacillus Subtilis gene atpD* identification, our goal is to demonstrate the implementation of robust microfluidic functions and an industrialization strategy. The key enablers for widespread acceptance of microfluidic products include assay robustness and minimal cost per test, careful consideration of system design, fabrication, assembly and hardware development. To address these issues with the proposed approach, we selected the materials, the fabrication means and assembly strategies which meet the requirements for further realistic industrialization. These aspects reinforce our efforts to work with low-costs thermoplastics and thermoplastic elastomers affording the ease of fabrication, enhanced bonding properties and biochemical surface modification.[15,16,17]

2. Materials and methods

2.1 CD architecture, design and biological components

The overall architecture of the proposed LoD consists of four distinct plastic elements including; a molded CD, a flat substrate, a microarray insert and a hybridization microfluidic chamber (figure 1). A 1.3 mm thick 120 mm diameter molded thermoplastic elastomer CD, containing channels and reservoirs of three different depths was sealed on a flat, 250 µm thin polycylic-olefin (PCO) substrate. Four identical sectors have been implemented for simultaneous independent detection. On the top surface of each sector, we positioned the microarray and the hybridization chamber which consisted of two parts of 0.5 mm thick plastic components having a 10×20 mm^2 surface area. The DNA microarray was spotted onto the flat biochemically modified PCO substrate. Two 1 mm diameter through-holes in TPE enable communication between the microarray positioned on the top of the TPE fluidic circuitry. The TPE fluidic part featured a microfluidic cavity for the hybridization reaction. The proposed miniaturized biochip required the loading of four types of liquid by pipetting: *i)* the raw sample, *(ii)* the PCR reagents, *(iii)* the exonuclease buffer and *(iv)* the washing buffer. The main

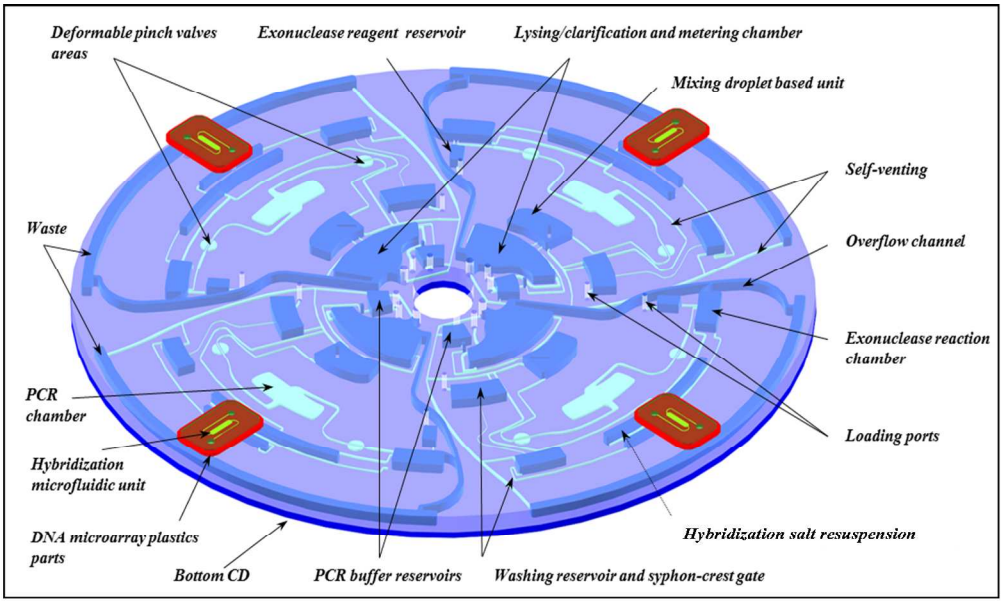

Fig. 1 Schematic of the disposable plastic device including four nucleic acid parallel tests for point of care NA diagnostic indicating lysis, clarification, PCR amplification, exonuclease reaction, microarray hybridization and washing functions.

biological functions are shown in the design schematic of Figure 1 and comprise (i) a lysis/clarification and metering unit, (ii) a lysate-PCR droplet based mixing unit, (iii) a PCR unit, (iv) an exonuclease unit, (v) a hybridization salt resuspension unit, (vi) a microarray hybridization unit, and (vii) a wash unit.

Lysis/clarification and metering unit. Starting from the inner portion of the CD, we implemented a lysis/clarification and volume metering chamber for the loaded sample. The lysis unit incorporated a magnetic circular disk and zirconium/silica beads. The circular disk was actuated by strategically placed permanent magnets on the stationary spinstand in order to produce bead collisions and inter bead shear flow capable of disrupting the cell membranes. This unit also performed the centrifugal elimination of solid contents and other cellular debris, and performed controlled transfer of clarified supernatant.

Lysate-PCR droplet based mixing unit. Next, a droplet-based mixing unit with deflectors for efficient mixing of the PCR reagents and the metered lysate was implemented (see section 2.2.2). The transfer of the liquid mixture into the PCR unit occurred via the bottom portion of the chamber in order to ensure robust and bubble-free filling. A capillary valve was used to stop the flow once the liquid reached the entrance of the exonuclease unit.

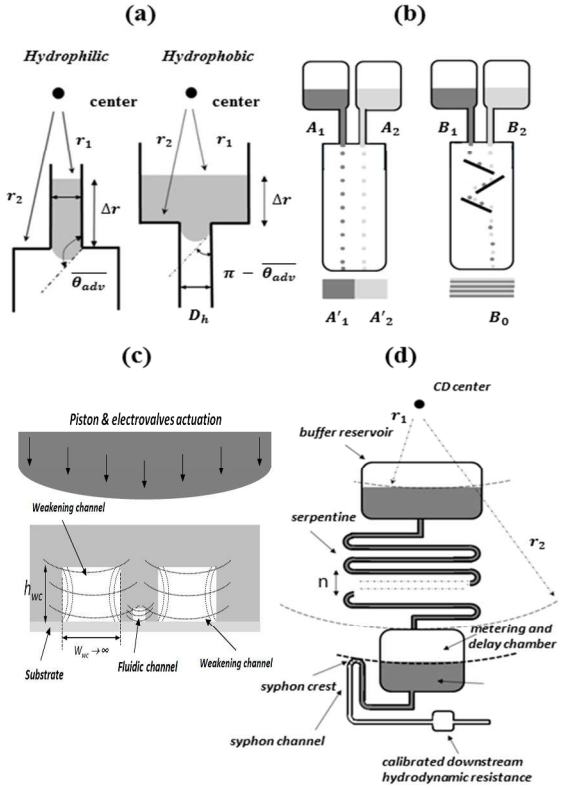

Fig. 2 **(a)** Schematic illustrations of hydrophilic and hydrophobic capillary valves. A sudden expansion of a microchannel represents the hydrophilic valve, while the hydrophobic valve is represented by a constriction. **(b)** Comparison of two passive microfluidic mixing mechanisms based on droplets approach, with and without a deflector structure in the chamber. **(c)** Schematic of a cross-sectional view of three channels illustrating pinch valving for PCR. A central channel displaying a 100×100 μm^2 square section area is completely deformed and closed due to the force generated by a piston. Neighboring 200 μm deep cavities improve the closing capabilities of the fluidic channel. **(d)** Schematic of timed valving approach. The rate of the flow from the reservoir to the delaying and metering chamber is controlled by the hydrodynamic resistance (serpentine channel). As the level of the liquid in the metering chamber reaches the siphon crest, the liquid is drained entirely through the siphon channel into the downstream microfluidic circuit.

PCR unit. PCR was performed by stopping the CD and applying vacuum through the integrated vacuum grooves on the CD platform ensuring good contact with the integrated Peltier elements. Pinch valves were employed to close the PCR chamber during thermal cycling (see section 2.2.4).

Exonuclease unit. Following PCR, the amplified sample was transferred into the exonuclease unit and mixed with exonuclease enzyme. In this unit, the mixing strategy employed was based on a back and forth motion of a single disc inserted in the reservoir (see section 2.2.2). It is noteworthy that the remaining upstream liquid was directly transferred into the waste chamber via the overflow channel.

Hybridization salt resuspension unit. Liquid transfer into a reservoir containing previously deposited dried hybridization buffer reagents was performed using a capillary valve positioned at the exit of the exonuclease unit. Downstream this reservoir, another capillary valve allowed the liquid to be maintained for rehydration purposes.

Microarray hybridization unit. The microarray hybridization unit is comprised of the microarray insert and the hybridization chamber position on the top CD surface. A higher spin frequency was employed to drive the liquid from the CD plane through the vertical access port into the microarray and the hybridization chamber.

Wash unit. In order to perform the final washing step, a wash reservoir was included which communicates with a downstream chamber connected to a siphon–like channel structure. This allowed the liquid to flow downstream in the retention intermediate reservoir chamber and finally to the wash-out the microarray. The decisive element for the accurate control of the washing step is the moment at which the liquid reaches the siphon crest structure and consequently enables downstream flow (see section 2.2.5).

2.2 Centrifugal microfluidic functions

2.2.1 Capillary valves

Capillary valves offer an attractive approach to control liquids on a CD platform. In addition to previously reported experimental works, we describe and broaden the analysis of the bursting conditions of capillary valves.[18,19] For a hydrophilic valve (Figure 2a), a sudden expansion of the microchannel traps the liquid meniscus, which is stopped at the valve entrance until the driving spinning force overcomes the resisting capillary force. By adapting the work of Cho *et al.*,[20] and considering a balanced advancing contact angle ($\overline{\theta_{adv}}$) accounting for the different fluidic and sealing materials used, and finally by including a correction factor for the rectangular hydraulic diameter,[21] the capillary burst frequency can be written as:

$$\omega^2 = \frac{\sigma \sin \overline{\theta_{adv}}}{\pi^2 \rho \Delta r \bar{r} D_h^{1.14}} \qquad (1)$$

where ω, σ, ρ are respectively the angular velocity, the surface energy and the liquid density, and Δr and $\bar{r}$ are respectively the

radial length occupied by the liquid, and the average distance of the liquid element from the CD center. D_h refers to the hydraulic diameter and describes a rectangular channel section of a width and height (w, h) equivalent to a cylindrical channel having a D_h diameter. For more details refer to the supplementary information (SI) section 1.1.

For a hydrophobic valve, a sudden decrease in the channel cross-section prevents the liquid from flowing downstream. Consequently, pressure is required to force the liquid to penetrate into the channel (Figure 3a). The resulting burst frequency (Eq. 2) can be obtained using pure geometrical considerations to compute the capillary force required for the liquid to flow through the valve:

$$\omega^2 = \frac{\sigma \cos(\pi - \overline{\theta_{adv}})}{\pi^2 \rho \Delta r \bar{r} D_h^{1.14}} \qquad (2)$$

2.2.2 Mixing elements

Two approaches were used for mixing. The first approach was based on convection using a solid movable disk in the mixing reservoir.[22,23] This method was used for the mixing of the exonuclease buffer with the post-PCR product, at a 1:4 volume ratio, respectively. A parylene coated magnetic disk 1.87 mm in diameter and 0.68 mm thick was introduced in the reservoir prior to bonding (VP 724, VP Scientific Inc., CA). An oscillating, shake-mode-mixing protocol was employed, in which fast changes in the rotation direction enhanced mixing by inertial and shear forces, resulting in turbulent and convective mixing. The mixing time was thus reduced from several minutes, typical for pure diffusion-based mixing, to several seconds. Additionally, a novel mixing method was developed for instantaneous mixing of two or more liquids. The concept is based on the mixing of droplets generated at the entrance of a reservoir. In Figure 2b, two liquids simultaneously pass from their respective supply channels into a large reservoir and the flow is fractionated into small droplets. If the droplets are released at points A_1 and A_2, they will fly in the radial outer direction and subsequently land at A'_1 and A'_2 positions respectively. The two liquids will accumulate on each half of the reservoir, as illustrated by the rectangle below the corresponding schematic in Figure 2b. In this case, limited by the single liquid interface, the resulting diffusive mixing is very weak. To overcome this limitation, we integrated deflection elements along the droplets pathway in order to deflect and force droplets to land at the same point B_0. In this case, the droplets stack on top of each other and form thin layers, thus significantly increasing the surface to volume ratio and practically mixing together instantaneously.

2.2.3 Flow rate in CD microfluidics

With only a few exceptions,[24,21] the lack of well-developed analytical tools that describe steady state flow on a CD platform, limits the ability to integrate complex on-board protocols that require numerous liquid handling steps and time-dependent liquid flow control. In this work, we propose a simple and general approach to treat the control of the flow rate on a CD. We simplify the linear density integral from the Navier-Stokes equation along a channel and consider the hydrodynamic resistances in correlation with the specific design parameters. This allows the expression of the total flow rate Q through the microfluidic circuit, consisting of a series of N channels of different cross-sectional areas $S_1, S_2, S_3, \ldots, S_N$ and different lengths $L_1, L_2, \ldots, L_N$ ending at positions r_1, r_2, ..., r_{N+1}, in the following form:

$$Q = \frac{\frac{1}{2}\rho\omega^2(r_{N+1}^2 - r_1^2)}{a + b} \qquad (3)$$

where the a and b terms represent the two major hydrodynamic resistance terms ($R_{hyd,j}$). The term a can be written as follows:

$$a = Max_{i=1}^{i=N}\left(R_{hyd,i}\right) = R_{hyd,j} = \frac{32\mu L_j}{h_j w_j D_{h,j}^2} \qquad (4)$$

where (h_j, w_j) represent the height and the width of the S_j rectangular channel cross section, section extended along L_j, and μ is the fluid viscosity. For more details and the complete derivation of equations (3) and (4), please referrer to the SI section 1.1.

2.2.4 Pinch valves

The elastomeric TPE layer integrated in the architecture of the LoD allowed the implementation of pinch valves in order to close and isolate the PCR chamber during thermal cycling. The pinch valves were actuated using two electro-valves actuated with a 150 kPa pressure source. The deformation and closing efficiency were optimized with the integration of microstructures surrounding the micro-channel to be closed. These additional micro-cavities ensured proper deformation of the channel corners in order to hermetically seal the channel. Figure 2c displays a cross-sectional schematic of the construct with related geometries. For more details, please referrer to the SI section 1.2.

2.2.5 Timed valving and delayed siphoning

In addition to capillary valves, a novel strategy for precise control of liquid delivery and flow was implemented. In this approach the wetting properties of the microfluidic channels play no role which renders the design more robust.[25] The proposed technique is based on the coupling of the following two elements: a hydrodynamic resistance designed as a serpentine channel and a siphoned chamber for delay and metering (Fig. 2d). The flow rate from the reservoir is simply controlled by the hydrodynamic resistance. Since the serpentine channel drains directly into the metering chamber, the filling time of this chamber is controlled by the geometry of the serpentine channel and the spinning protocol. Once the liquid in the chamber attains the critical level corresponding to the priming of the siphon crest, the liquid is flushed into the downstream microfluidic circuit. Due to the spinning dependency of the flow rate, the delivery of the washing buffer at an exact time t_{wash} required precise control of the delay chamber filling. The flow rate was calculated using equation (3), by additionally performing the integration over the different angular velocity ω. Finally, for a metering chamber filled with a certain volume V_{wash} the crest is reached at a time t_{wash} which depends on the flow rate Q, as shown in the following expression:

$$V_{wash}(t_{wash}) = Q(t,\omega).t_{wash}$$

$$V_{wash}(t_{wash}) = \frac{\rho(r_2^2 - r_1^2)}{2(a+b)} \int_0^{t_{wash}} \omega^2(t)dt \quad (5)$$

2.3 Fabrication and assembly

Complete LoD fabrication and assembly procedures are provided in the SI section 1.3. Briefly, the CD microfluidic circuit and the microfluidic hybridization chambers were fabricated in styrenics TPE block-copolymers material using hot embossing and an epoxy mold. The final shaping of all TPE components was accomplished with a dedicated cutter/puncher tool for the precise definition of the CD shape and through-hole structures. The bottom CD substrate consisting of polycyclic-olefin (PCO) polymer (Zeonor 1060R, Zeon Chemicals, Louisville, KY) was fabricated by injection molding in the form of a flat disk. The top flat DNA microarray PCO components were also injection molded. They were subsequently spotted with specific oligomers (Integrated DNA Technologies, Inc., Coralville, Iowa) using a previously published procedure.[26] Prior to bonding and assembly, reagents and magnets were dispensed into specific CD units (see section 2.4). The mechanical properties of the TPE promoted an intimate contact of the CD with the thin PCO substrate, leading to a perfect but reversible seal of the two thermoplastic surfaces. To achieve permanent bonding, a heating step of 70 ºC for 2 hours was simply performed in a standard oven. Finally the assembly was achieved by placing the TPE hybridization chambers and the spotted PCO microarrays on the top CD surface.

2.4 Integration of liquid solution and solid reagents on the CD

To demonstrate the robustness of the platform, gram positive bacterial spores were used as representatives of organisms difficult to lyse. *Bacillus atrophaeus* subsp. *globigii* (Bg) spores strain CCRI-9827 were sporulated according to the procedure detailed by Laflamme *et al.*.[27] The assay was performed using a 90–120 µl DI water sample containing a concentration of 1000 spores•mL^{-1}. A 10 µl of PCR reagent containing 1 µM Cy3-Bg-specific forward primers, 1 µM phosphated Bg-specific reverse primers, 2.5 mM $MgCl_2$, 3.3 g.L^{-1} bovine serum albumin, 200 µM deoxynucleoside triphosphate, 50 mM KCl, 10 mM Tris-HCl, 0.1% Triton X-100 and 0.2 U Taq (Promega, Madison WI), was pipetted onto the CD. Subsequently, 4 µl of 1X Lambda-exonuclease reaction buffer (New England Biolab Inc., Ipswich, MA) was pipetted onto the CD for selective digestion of the reverse amplicon strand.[28] The washing step was performed using a 20 µl solution of 0.2×SSPE (Saline Sodium phosphate EDTA) + 0.1% sodium dodecyl-sulfate. In each lysis chamber, prior to CD bonding, an aliquot of 60 µl lysis-bead slurry consisting of 150 µm diameter zirconium/silica beads (BioSpec Products, Inc., OK) suspended in a 1% (w/w) solution of polyvinylpyrrolidone in DI water was pipetted. Subsequently, the slurry was dried at 70 ºC for 20 min, resulting in compact bed-bead covering nearly two thirds of the lysis chamber. Four pre-autoclaved ferromagnetic discs with a 5.13 mm diameter and 0.63 mm in thickness were then positioned into the chamber on top of the beads. During the thermal treatment of the lysis-bead slurry, 18 µl aliquots of hybridization buffer (1×TE buffer in a 1 M NaCl aqueous solution) were also dried in the resuspension chambers resulting in crystalline salts. Finally four ferromagnetic discs, similar to that used for lysis, were added into the exonuclease reaction units for mixing purpose.

2.5 Bioassay CD protocol

Figure 3 details the 15-step spin program for the complete NA assay with various spin frequencies and the corresponding step durations. The NA assay starts with lysis in the lysing chamber, which involves a magnetically actuated bead-beating

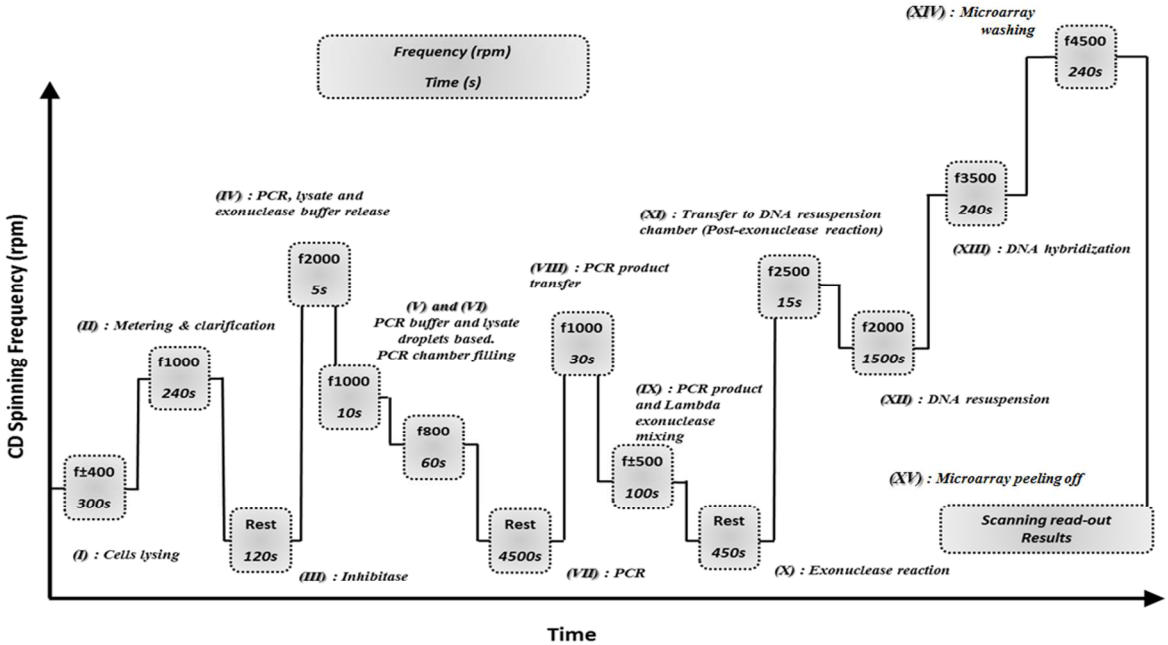

Figure 3 The spinning CD protocol including fifteen steps for nucleic acid detection.

lysis protocol.[29,13,30] Lysis was performed according to the spin profile shown in step I of Figure 3 with an oscillation period of 10 sec. Step II represents a clarification step, wherein cellular debris present in the solution is separated, leaving nucleic acid suspended in the supernatant. Step III required the CD to be stopped, and vacuum-enhanced contact with the Peltier element to be established followed by a 2 min heating at 95 ºC to inactivate the PCR inhibitors. At step IV, the CD spinning frequency was increased to 2000 rpm for 5 sec to open the valves (V_1, V_2 and V_4) holding the PCR, supernatant and exonuclease solutions, respectively. Subsequently, the CD velocity was successively reduced in order to ensure efficient droplet-based mixing and a bubble-free homogenous filling of the PCR unit (step IV and V). At 800 rpm, 20 µl of mixed PCR/supernatant (1:1 ratio) stopped at V_3. A fraction of this volume (8 µl out of the 20 µl) stayed between the exit of the mixing chamber and V_3, while the remaining volume (12 µl) was held in the mixing unit. Meanwhile, an additional 20 µl volume of pure (*i.e.* un-mixed) supernatant entered the mixing unit, as V_2 was designed at a radial level position, which allowed for a total transferred volume of 30 µl. This liquid reserve is of paramount importance for the assay integration, as it ensures, in concert with the liquid remaining in the in-coming PCR channel, the integrity of the liquid column height required to efficiently push-out the amplified sample from the chamber. Without this liquid reserve, the chaotic formation of bubbles in the PCR chamber would interrupt the liquid continuum on the CD microfluidic circuitry, ultimately leading to device failure. For the PCR amplification described in step VII, the CD was again stopped to allow for the vacuum-enhanced contact with the Peltier element. The PCR chamber was isolated by actuating the pinch valves and the PCR amplification was performed with the following thermal cycle protocol: 180 s at 94 °C, followed by 45 cycles of three steps consisting of 10 s at 95 °C for denaturation, 30 s at 56.5 °C for annealing, and 30 s at 72 °C for extension. Air bubbles were generated during thermal cycling, however, following the opening of the pinch valves and resuming CD spinning, the liquid was driven to the bottom of the PCR unit, while the air bubbles accumulated in the chamber, merged and generated a single air pocket at the top portion of the chamber. At step VIII, upon resuming the CD spinning, V_4 was opened, and a total volume of 16 µl, containing 6 µl of the amplified sample, entered the exonuclease unit containing the exonuclease reagent. The mixing of the amplified sample and exonuclease reagents in step IX was performed using a rapid oscillation of the disc. Then, in the rest position, the exonuclease digestion was performed for 10 min at room temperature (step X). Next, at a spin speed of 2500 rpm the capillary valve V_5 was opened, and the liquid entered a reservoir containing the dried DNA buffer reagents (step XI). The spinning frequency was then reduced, and the liquid entered the resuspension reservoir (step XII). At step XIII, the frequency increase opened the capillary valve V_6 and the liquid flowed towards the microfluidic hybridization chamber. Finally, with our timed valving strategy, the washing solution flowed through the hybridization chamber (step XIV). Following the hybridization reaction, the hybridized microarray was removed from the TPE hybridization unit and scanned for optical reading (step XV).

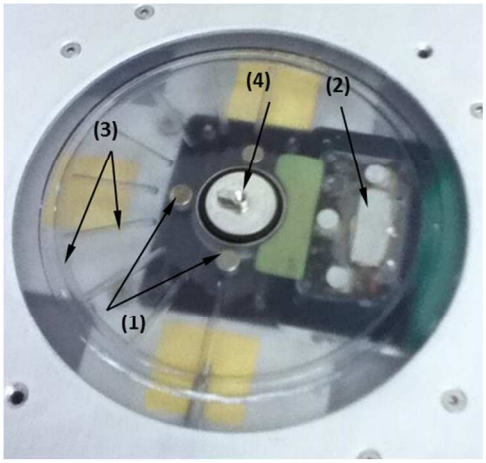

Fig. 4 A photograph of the hardware platform including *(1)* magnetic elements for cellular lysing, *(2)*, heating and cooling Peltier elements, and *(3)* vacuum-contact capabilities. Stationary platform is motorized and includes a step by step controller for CD positioning. Platform integrates a *(4)* z-motorized axis to accommodate CD and platform gap distance for magnetic coupling and decoupling.

2.6 CD Hardware platform

We conceptualized and developed a computerized centrifugal test setup with the collaboration of Phasiks Inc. (Los Alamitos, CA, USA). The setup was controlled with a LabVIEW program and comprised a fully motorized stage, a strobe, a camera and several Peltier heating/cooling elements. In Figure 4, we show a view of the hardware platform with its integrated active mechanisms: *(1)* permanent magnets for cell lysing, *(2)* Peltier elements for PCR, *(3)* machined groove on the surface of the plastic platform connected to a vacuum source for efficient thermal contact, and *(4)* a z-motorized axis to accommodate the CD/platform gap distance

3. Results and discussion

3.1 CD fabrication and characterization

The materials for the fabrication of the CD platform were selected by considering bio-compatibility, surface properties, as well as ease of fabrication, assembly and bonding. The advantages of TPE materials in terms of costs, enhanced molding capabilities and convenient bonding properties (from low pressure to no pressure at moderate temperatures) were already discussed.[15-17] These benefits offer synergetic and simultaneous solutions for both the POC prototyping development phase and the product development from the starting point to the end. Unlike PDMS, which requires pre-compounding and degassing prior to each use, TPE can be extruded in sheets and rolled onto a mandrel for later use (Fig. 5a). For prototyping purposes, we employed a fabrication strategy that enabled rapid thermal molding of TPE devices using a low-cost epoxy mold in a hot-embossing process. Thus, hundreds of device copies can be obtained in one week. Figure 5b and c show the epoxy mold and the assembled CD device, respectively. The initial multilevel SU–8 patterning step for the pre-mold fabrication was intentionally limited to three levels and to aspects ratio structures below 1.7. These design criteria match the currently feasible high quality

metallic mold fabrication processes and provide for the possibility of fabrication of an electroformed metallic mold for future production-level device fabrication. Figures 5d-f show scanning electron microscope images of the embossed structures, demonstrating well-defined shapes and excellent surface quality (see also SI section 2.1). Atomic force microscopy phase mode imaging was used to observe the detailed morphology of the biphasic nature of the TPE material (Fig. 5g). A first phase consists of hard polystyrene (PS) nanometer cluster (10-30 nm) domains, which are 3D organized and distributed in an 85% rubber matrix of (ethylene-butylene) (EB). This morphology provides the basis of the material performance: rigid PS domains act as junction points that stabilize the polymer matrix, while the EB dominant phase offers elastomeric properties. In addition, the size and cluster distributions promote the uniformity and homogeneity of the TPE surface at the microfluidic device scale level. This morphology provides stable elastomer properties from –40 ºC to 110 ºC, offering a large spectrum of operational temperatures compatible with a wide range of biological reactions. Figures 5h and 5i show respectively, a sector of a CD bonded and assembled with all plastics components and the TPE microfluidic hybridization chamber filled with a red colored solution placed over the CD and covered with a rectangular PCO insert.

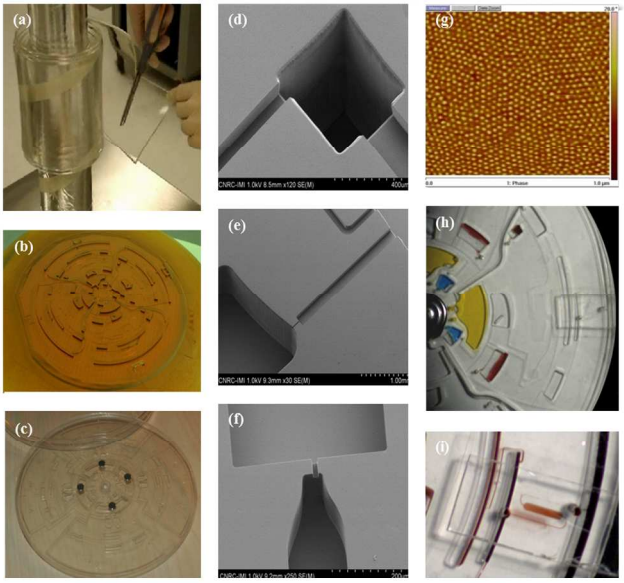

Fig. 5 **(a)** A photograph of an extruded TPE foil on a roll from which pieces can be conveniently cutted before use. **(b)** A photograph of epoxy based master mold for hot embossing and injection molding replication. **(c)** A photograph of an assembled TPE hybrid CD including magnetic discs for lysing purpose. **(d)-(f)** Series of SEM micrographs showing hot-embossed SEBS CD layer displaying reservoirs, microchannels and capillary valves. **(g)** Contrast phase AFM image of SEBS molded surface illustrating the blocked structure morphology of the TPE material. The white areas (10–30 nm) correspond to the polystyrene clusters distributed in a dominant elastomeric ethylene/butylene soft phase. **(h)** An optical image showing one sector of the CD loaded with four food colorants for illustration purpose. **(i)** A close-up view of the microfluidic hybridization chamber covered with a microarray filled with a red dye solution.

3.2 Microfluidic properties and characterization

In order to synchronize all the steps of the complex biological protocol, we had to ensure the stringent control of capillary valves operation, as well as the control of flow rates and their respective timing. Table 1 displays the critical dimension, calculated values and experimental data of all capillary valves and liquid transfer rates involved in the system. For capillary valve structures, the estimated level of accuracy ranged from 78 to 93% for the first five valves, while a larger deviation from theory was observed for the final V_6 valve. This is attributed to the fact that the liquid column height Δr is excessively small for this given reservoir (Fig. 2a) and as such is subject to variation on the precision of volume definition. CD wobbling is also more prominent at this radial position in comparison with other valves, distributed closer to the CD center. Additionally, interdependence and correlation aspects represent significant issues concerning the level of robustness for CD operation. Specifically, the presence of several rest periods and instances where microfluidic units are empty induce the de-correlation of capillary valves, with exception of V_1 and V_2 with respect to V_3. Specifically, V_1 *and* V_2 delivered the sample supernatant and the PCR liquid buffer, respectively, while V_3 functioned as a stop gate preventing the liquid from entering the exonuclease unit. This is the reason behind the intentional reduction of the CD spinning rate during the mixing and PCR chamber filling periods. Finally, for the entire capillary valve series, confidence intervals ranged from 3σ to 5.3σ offering a high level of operating precision and robustness. The second part of table 1, shows the properties of each liquid transfer (T_i) in concert with the theoretical values calculated with equation (3). For all CD fluidic transfers, a high level of accuracy in the range of 94 to 99% has been established, except for the transfer T_4. This precision was reached through a proper characterization and dimensional stability of the molded CD microfabrication process, wherein the critical dimensions *(w,h,l)* were precisely characterized along with their respective shrinkage coefficients. The transfer T_4, diverged significantly from the model, which can be explained by the significant variation of the experimental r_1 value over the duration of this transfer. Consequently, contrary to the model, this value cannot be considered constant over time. Therefore, the exact value was characterized experimentally and the protocol was adjusted accordingly.

Figure 6 demonstrates the assay integration and specific fluid pathways. Figure 6a illustrates the complete and fully loaded CD. Figure 6b, demonstrates the mixing efficiency based on the droplets method. Temporally controlled and synchronized droplets composed of 10 µl blue PCR buffer and 10 µl of metered yellow clarified lysate buffer entered the mixing unit at an identical flow rate. The image insert shows the deflector structure performing droplets fragmentation and orientation. The accumulation of the liquid and appearance of the green color at the bottom of the mixing unit illustrate the efficiency of the mixing. Subsequently, mixed species entered the PCR chamber via a channel path indicated by a dashed arrow. High quality and bubble-free filling was routinely observed. Those filling properties are of paramount importance as they are related to any air expansion upon PCR thermal cycling and are of general concern for all centripetal microfluidic platforms.[31,32] In order to

Capillary Valves @ V_i Transferts T_j : @rpm/volume(µl)	Critical dimension (w,h,l) (µm,µm, mm)	Calculation V_i : rpm T_j : $Q(\mu l.min^{-1})$	Experiments V_i : x_{mean} ± σ (rpm) T_j : $Q(\mu l.min^{-1})$	Theory fit (%)
V_1 @ Lyse	(70, 100)	1152	1248 ± 118	91%
V_2 @ PCR buffer	(200, 100)	1439	1545 ± 73	93%
V_3 @ Incoming exonucl	(11,20)	1506	1720 ± 82	86%
V_4 @ Exonucl. buffer	(20,20)	1173	1480 ± 67	78%
V_5 @ Outcoming exonucl.	(30,20)	2246	2460 ± 142	91%
V_6 @ DNA buffer	(10,20)	3224	4150 ± 197	71%
T_1 : Lysate@1500/(30)	(35,100,2.3)	17.4	18.1	96%
T_2 : PCR buffer@1500(10)	(35,100,3.0)	24.5	25	97%
T_3 : Amplif. to exonucl.@1500/(40)	(17,20,0.04)	6.3	6.5	96%
T_4 : Exonucl. to Resuspension@2000/(20)	(12,20,0.15)	6.7	1.2	18%
T_5 : Hybridization@3500/(20)	(14,20,2.0)	4.8	4.9	99%
T_6 : Temporization washing loop	(43,20, 20.6)	0.44 (1)	0.41	95%
T_7 : Washing@4000/(20)	(14,20,2.0)	6.3	6.2	94%

Table 1 Critical dimension, calculated values and experimental data of all capillary valves and liquid transfer involved in the system.

sustain PCR operability and close the PCR chamber during thermal cycling, we implemented pinch valves which exploit the deformable and elastomeric capabilities of TPE.[17,33,34] Images shown in Fig. 6c$_1$ and 6c$_2$ illustrate the electro-valves and tubing connections positioned above the CD. Fig. 6c$_2$ displays the image of the chamber after 45 PCR cycles and 10 sec CD spinning at 1000 rpm showing the details of liquid repositioning at the bottom of the chamber upon spinning. Figure 6d, illustrates post-PCR liquid transfer inside exonuclease reaction chamber. A 20 µl volume of sample supernatant flowed downstream through the mixing unit and subsequently entered the PCR chamber in order to push-out and transfer the amplified green liquid to the exonuclease reaction reservoir. Unamplified yellow liquid was then contained in the PCR unit, while the green solution was transferred. In the exonuclease unit, an overflow channel performed metering of the exonuclease liquid reagents. Following the exonuclease reaction, the capillary valve V_5 was opened and the green sample flowed toward the hybridization buffer resuspension unit as illustrated in Figure 6e. The image insert shows the crystals resulting from the drying of the reagents. Finally, Figure 6f displays homogenous filling and washing of the microarray inserts with the red-colored washing buffer. It was

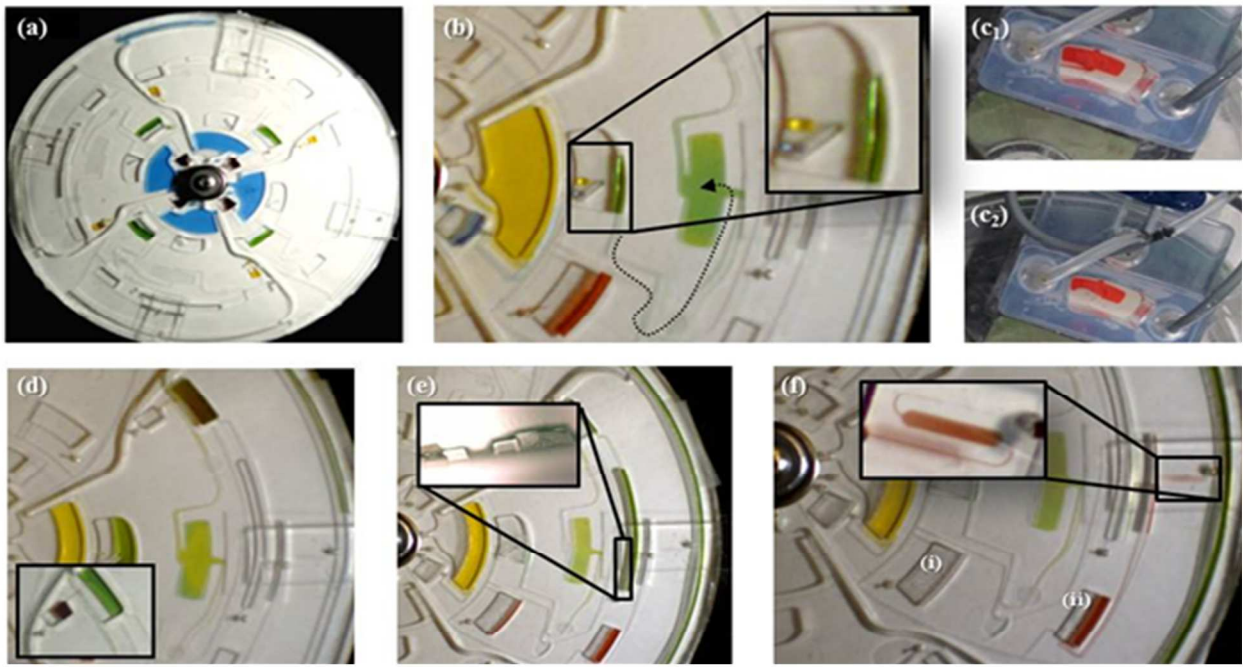

Fig. 6 A series of stroboscopic pictures illustrating, **(a)** A microfluidic CD holding four parallel NA tests **(b)** An illustrative photograph of droplets based mixing and PCR chamber filling. **(c$_1$) , (c$_2$)** The pinch valve hardware and de-bubbling properties of PCR unit after thermocycling when spinning has been resumed. **(d)** The PCR product transfer, metering and mixing with 4 µl of lambda exonuclease reagent in the exonuclease reaction unit. The inserted image shows the brown lambda reagent prior to its transfer to the green PCR product. **(e)** The transfer of digested and metered 20 µl volume of amplified product into the chamber that contains crystalline buffer salts highlighted in the image insert. **(f)** The flow of the red colored washing buffer solution through the microfluidic hybridization chamber and over the microarray unit

observed that the washing buffer reservoir *was emptied (i)* while the intermediate delay chamber was filled with the liquid reaching the crest for downstream transfer *(ii)*. Homogenous filling of the chamber was achieved via the bottom portion of the microfluidic unit, using the identical microfluidic path employed for the previous hybridization step. The robustness and the operating efficiency were indubitably ensured by the stringent control of all flow times, flow rates, flow filling modes and liquid transfer procedures. No significant variations or unstable liquid flow events such as filling failures, liquid continuum break-up, and flow de-synchronization were observed. All thermal and mechanical constraints related to various microfluidic procedures were aligned with fabrication materials and methods. This allowed robust bio-assay implementation with precise control of all components. It is noteworthy that while the capillary valve positioned at the entrance of the exonuclease unit represents the weakest system component (a 3.3σ characteristic), the possibility of fluid flow control failure is relatively small (0.1%).

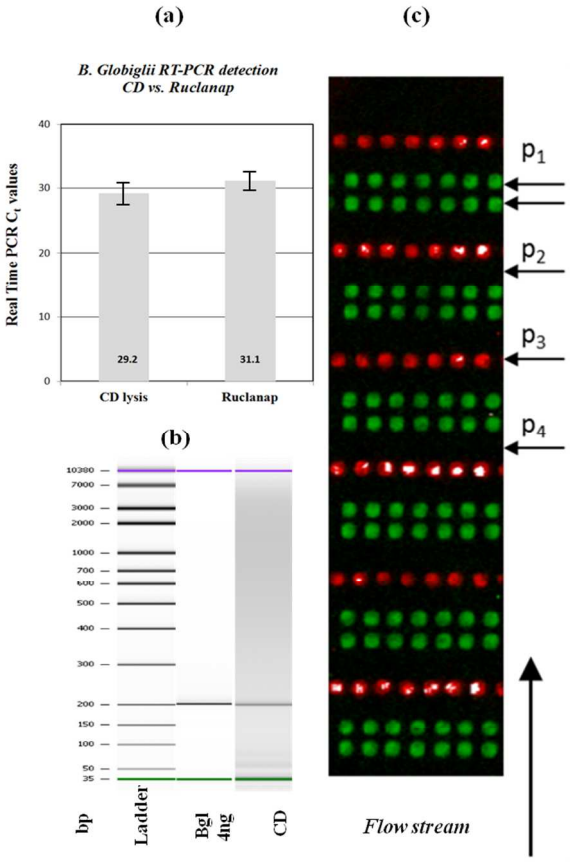

Fig. 7 **(a)** The comparison of bacterial spore lysis efficiency between the CD platform and commercial bead-beating kit (BD GeneOhm™ Lysis Kit). Real-time PCR amplification levels are expressed as cycle threshold values (lower value indicates higher lysis efficiency). **(b)** The amplification of *Bacillus atropheus* atpD gene. The 210 bp band demonstrates the efficient amplification for 100 copies. **(c)** A fluorescence microscope image of microfluidic microarray hybridization. Three species-specific capture probes targeting *B. Globiglii* spore sequences were employed. The array displays two consecutive lines of Cy3-labeled (A-S-caoAthH1507) positive control (p_1), followed by a Cy3-labeled (A-S-34V31020LinfH435) negative control (p_2) and a Cy5-labeled (A-S-bbc2) positive control (p_3) (white pixels indicate signal saturation) and a blank line (p_4).

3.3 *Demonstration of B. atropheus CD Lab nucleic acid assay*

The efficiency of cell lysis function implemented on the CD platform was demonstrated using bacterial spores (Fig. 7a) and compared to the commercially available bead-beating kit (BD GeneOhm™ Lysis Kit). Herein, the CD was subjected to the previously described protocol steps I, II and III (see figure 3). A volume of pure supernatant was transferred downstream and 20 µl has been collected. For both, the commercial kit and the CD lysis method, a volume of 2 µl was subjected to real-time PCR. Lysates containing 2000 lysed spores were amplified in a 25 µL volume. Real-time PCR assay was performed using specifications from a previously reported protocol.[35] The resulting C_t values for both methods were statistically identical, thus validating the lysis function efficiency of the CD platform. Therefore, the sample preparation feature of our LoD could potentially allow for a wide range of microorganisms to be analysed. PCR amplification was validated by the amplification of 100 copies of *B. atropheus gene atpD* (210bp region). The PCR chamber was characterized using thin wired thermocouples that were positioned within the PCR unit and the aluminium Peltier elements (at a distance of 1.5 mm) in order to investigate the temperature off-set and ramp rates. For the denaturation, annealing and extension steps, the temperature off-sets corresponded to 11.5, 1.2 and 5.8 °C respectively, and heating and cooling rates of +1.4 °C.s^{-1} and -2.1 °C.s^{-1} respectively, were determined. Finally, the temperature profile inside the chip was set to 10 s for denaturation and 30 s for both annealing and extension at 95, 56.5 and 72 °C respectively. In total, 45 cycles were performed within 88 minutes, from which 42% of the time was dedicated to temperature transition. Prior to thermal cycling, a hot-start (95 °C for 3 min) was conducted. Upon completion of the amplification, the pinch valves were removed, and the CD was spun at 1000 rpm for 30 seconds. This allowed the transfer of the PCR products to a downstream reservoir from which 1.0 µl was extracted and injected into an Agilent Bioanalyser 2100 cartridge for detection. A visible band on the agarose gel indicated successful LoD PCR amplification (Fig. 7b). The 210 bp band demonstrated the efficient amplification of the target gene and a well-controlled specificity. Finally, the complete fifteen-step assay was validated. Figure 7c, shows a fluorescent microscope image of an array of 7 × 30 spots obtained by recombination of Cy3 and Cy5 channels. The hybridization was carried out for 4 min at room temperature with 20 µl of amplified and digested sample, and subsequently washed-out with SSPE washing buffer for 4 min. Three species-specific capture probes targeting *B. atropheus* spores sequences were employed. The array displayed two consecutive lines of Cy3-labeled positive control (p_1), followed by a Cy3-labeled negative control (p_2), a Cy5-labeled positive control (p_3) and a blank line for evaluation of non-specific binding events (p_4). The fluorescence emission was confined to the spotted and hybridized areas and contrasted well with the bare plastic substrate. The fluorescence intensity decreased from bottom to top for p_1 and p_3 probes which occurred systematically for all arrays produced with this particular design and resulted from the depletion effects occurring along the fluidic stream.

4. Conclusion and perspectives

We have developed a complete fifteen steps nucleic acid assay utilizing novel methods for centripetal mixing and timed valving implemented on a CD designed for accurate control of fluid transfer, chamber filling modes and timing procedures. To the best of our knowledge, this is the first reported centripetal LoD capable of performing a complete molecular assay offering full spectrum of biological steps. Specifically, lysing, metering, clarification, PCR amplification, digestion, and microarray hybridization have been successfully integrated. In this report, we have demonstrated the NA detection of *Bacillus atropheus* as a model system. Furthermore, in comparison to the previously reported real-time PCR centripetal system,[36] the incorporation of microarray detection in the present LoD represents a higher level of integration and offers the possibility to accommodate a variety of biological assays on-CD. Furthermore, the CD can be adapted to handle different PCR reactions in the four PCR chambers for multiplexing purposes. In terms of the CD fabrication and assembly, the TPE material offers high quality and low density defect microstructuration capabilities. Simple, fast and reliable TPE bonding methodology further highlights this material as an important and adequate solution that meets the requirements of the early prototyping and bio-assay protocol development (quick iterations) and also of the potential final application. Due to the high complexity of the LoD NA assay development, the appropriate choice of material solution is of tremendous importance. The selected material needs to meet simultaneously the requirements of microfabrication, bonding and assembly, as well as to accommodate integration of reagents and biological samples. Hence, this paper demonstrates a seamless strategy that promotes a transfer path from prototyping toward industrialization based on TPE material solution. Future work is geared towards the biological demonstration of the complete NA assay including a 400 spots microarray. This assay will cover 99% of respiratory infections including, DNA and RNA viruses, bacteria and spores.

5. Acknowledgment

We thank our colleagues Hélène Roberge, François Normandin and Marthe Bernier for technical assistance, and we are grateful to Kyle Chrystal and Richard Welle for the CD platform development. This work was supported in part by the National Research Council of Canada, the US department of Health and Human Services, Genome Québec and Genome Canada.

Notes and references

1 H. A. Stone, A. D. Stroock and A. Ajdari, *Annu. Rev. Fluid. Mech.*, 2004, **36**, 381–411.
2 Lab on a Chip, a series of insight review articles in *Nature*, 2006, **442**, 367–418.
3 T. M. Squires and S. R. Quake, *Rev. Mod. Phys.*, 2005, **77**, 977–1026.
4 C. D. Chin, V. Linder and S. K. Sia, *Lab Chip*, 2007, **7**, 41–57.
5 W. Fisher, C. B. Cline and N. G. Anderson, *Anal. Biochem.*, 1964, **9**, 477–482.
6 N. G. Anderson, C. Yrice, W. Fisher, R. Canning and C. Burger, *Anal. Biochem.*, 1964, **7**, 1–9.
7 N. Anderson, *Science*, 1969, **166**, 317–324.
8 D. Mark, S. Haeberle, G. Roth, F. von Stetten and R. Zengerle, *Chem. Rev. Soc.*, 2010, **39**, 1153–1182.
9 R. Gorkin, J. Park, J. Siegrist, M. Amasia, B. S. Lee, J.-M. Park, J. Kim, H. Kim, M. Madou and Y.-K. Cho, *Lab Chip*, 2010, **10**, 1758–1773.
10 B. S. Lee, Y. Lee, H.-S. Kim, T.-H. Kim, J. Park, J.-G. Lee, J. Kim, H. Kim, W. G. Lee and Y.-K. Cho, *Lab Chip*, 2011, **11**, 70–78.
11 M. Focke, F. Stumpf, B. Faltin, P. Reith, D. Bamarni, S. Wadle, C. Muller, H. Reinecke, J. Schrenzel, P. Francois, D. Mark, G. Roth, R. Zengerle and F. von Stetten, *Lab Chip*, 2010, **10**, 2519–2526.
12 H. Kido, M. Micic, D. Smith, J. Zoval, J. Norton and M. Madou, *Colloids Surf., B: Biointerfaces*, 2007, **58**, 44–51.
13 G. Jia, K.-S. Ma, J. Kim, J. Zoval, R. Peytavi, M. G. Bergeron and M. Madou, *Sens. Actuators B*, 2006, **114**, 173–181.
14 M. Grumann, M. Dube, O. Gutmann, S. Lutz, J. Steigert, L. Riegger, K. Mittmann, M. Daub, R. Zengerle and J. Ducrée, in Proc. *in MicroTAS*, ed. A. Van Den Berg and P. Bergveld, Kluwer Academic Publisher, 2005, 328–330.
15 E. Roy, M. Geissler, J.-C. Galas and T. Veres, *Microfluid. Nanofluid.*, 2011, **11**, 235–244.
16 D. Brassard, L. Clime, K. Li, M. Geissler, C. Miville-Godin, E. Roy and T. Veres, *Lab Chip,* 2011, **11**, 4099–4107.
17 E. Roy, J.-C. Galas and T. Veres, *Lab Chip*, 2011, **11**, 3193–3196.
18 J. M. Chen, P.-C. Huang and M.-G. Lin, *Microfluid. Nanofluid.*, 2007, **4**, 427–437.
19 T.-S. Leu and P.-Y. Chang, *Sens. and Actuators A*, 2004, **115**, 508–515.
20 H. Cho, H.-Y. Kim, J. Y. Kang and T. S. Kim, *J. Colloid. Interf. Sci.*, 2007, **306**, 379–385.
21 M. Madou and G. Kellogg, *in Proc. SPIE Systems and Technologies for Clinical Diagnostics and Drug Discovery*, ed. G. E. Cohn and A. Katzir, San Jose, CA. USA, 1998, 80–93.
22 J. Steigert, M. Grumann, T. Brenner, K. Mittenbuhler, T. Nann, J. Ruhe, I. Moser, S. Haerberle, L. Riegger, J. Riegler, W. Bessler, R. Zengerle and J. Ducrée. *J. Assoc. Lab. Autom*., 2005, **10**, 331–341.
23 S. Lutz, V. Reitenbach, D. Mark, J. Ducrée, R. Zengerle and F. von Stetten, in Proc. *in MicroTAS*, ed. A. Van Den Berg and P. Bergveld, Kluwer Academic Publisher, 2008, 748–750.
24 D. C. Duffy, H. L. Gillis, J. Lin, N. F. Sheppard and G. J. Kellogg, *Anal. Chem.*, 1999, **71**, 4669–4678.
25 L. Clime, M. Mounier, E. Roy and T. Veres, In WO International application 2013003935 A1 and US provisional application 61/504,273, *Valveless centrifugal microfluidic platform and method for performing biological assays therein*. (2013).
26 G. A. Diaz-Quijada, R. Peytavi, A. Nantel, E. Roy, M. G. Bergeron, M. M. Dumoulin and T. Veres, *Lab Chip*, 2007, **7**, 856–862.
27 C. Laflamme, S. Lavigne, J. Ho and C. Duchaine, *J. Appl. Microbiol.*, 2004, **96**, 684–692.
28 K. Boissinot, A. Huletsky, R. Peytavi, S. Turcotte, V. Veillette, M. Boissinot, F. J. Picard, E. A. Martel and M. G. Bergeron, *Clinic. Chem.*, 2007, **53**, 2020–2023.
29 J. Kim, S. H. Jang, G. Jia, J. Zoval, N. A. Da Silva and M. Madou, *Lab Chip*, 2004, **4**, 516–522.
30 J. Siegrist, R. Gorkin, M. Bastien, G. Stewart, R. Peytavi, H. Kido, M. Bergeron and M. Madou, *Lab Chip*, 2010, **10**, 363–371.
31 H. Kido, M. Micic, D. Smith, J. Zoval, J. Norton and M. Madou, *Colloid. Surf. B*, 2007, **58**, 44–51.
32 J. Siegrist, M. Amasia, N. Singh, D. Banerjee and M. Madou, *Lab Chip*, 2010, **10**, 876–886.
33 T. Fatanat Didar, K. Li, M. Tabrizian and T. Veres, *Lab Chip*, 2013, **13**, 2615–2622.
34 M. A. Unger, H. P. Chou, T. Thorsen, A. Scherer and S. R. Quake, *Science*, 2000; **288**, 113–116.
35 F. Picard, M. Gagnon, M. Bernier, N. Parham, M. Bastien, M. Boissinot, R. Peytavi and M. G. Bergeron, *J. Clin. Microbiol.*, 2009, **47**, 751–757.
36 M. Focke, F. Stumpf, G. Roth, R. Zengerle and F. von Stetten F, *Lab chip*, 2010, **10**, 3210–3212.